

On the origin of cold-dense plasmas in the dusk magnetotail plasma sheet: MMS Observations

M. N. Nishino¹, Y. Saito¹, H. Hasegawa¹, N. Kitamura², Y. Miyashita³, T. Nagai¹, S. Yokota⁴,
D. J. Gershman⁵, C. T. Russell⁶, B. L. Giles⁵

¹Institute of Space and Astronautical Science, Japan Aerospace Exploration Agency

²Graduate School of Science, The University of Tokyo

³Korea Astronomy and Space Science Institute

⁴Graduate School of Science, Osaka University

⁵Goddard Space Flight Center, NASA

⁶University of California, Los Angeles

Key Points:

- MMS observed the cold-dense plasma sheet in the dusk magnetotail under the strongly northward IMF.
- Energy dispersions of the low-energy ions in the field-aligned direction were identified.
- Magnetic reconnection in the Kelvin-Helmholtz vortices near the magnetopause is a possible mechanism of generating the energy dispersions.

Corresponding author: Masaki N. Nishino, nishino@stp.isas.jaxa.jp

18 Abstract

19 The near-Earth plasma sheet becomes cold and dense under the northward interplanetary
 20 magnetic field (IMF) condition, which suggests entry of solar wind plasma into the mag-
 21 netosphere across the magnetopause. The cold and dense characteristics of the plasma
 22 sheet are more evident in the magnetotail flank regions that are interface between cold so-
 23 lar wind plasma and hot magnetospheric plasma. Several physical mechanisms have been
 24 proposed to explain the entry of solar wind plasma across the magnetopause and resultant
 25 formation of the cold-dense plasma sheet (CDPS) in the tail flank regions. However, trans-
 26 port path of the cold-dense plasma inside the magnetotail has not been understood yet.
 27 Here we present a case study of the CDPS in the dusk magnetotail by Magnetospheric
 28 Multiscale (MMS) spacecraft under the conditions of the strongly northward IMF and the
 29 high-density solar wind. The ion distribution function consists of high- and low-energy
 30 components, and the low-energy one intermittently shows energy dispersion in the direc-
 31 tions parallel and anti-parallel to the local magnetic field. Considering the time-of-flight
 32 effect of the energy-dispersed low-energy ions, we infer that these ions originate in the
 33 region down the tail, and move along the magnetic field toward the ionosphere and then
 34 come back to the magnetotail by the mirror reflection. The pitch-angle dispersion analysis
 35 gives consistent results on the travelling time and path length of the energy-dispersed ions.
 36 Based on these observations, we discuss possible generation mechanisms of the energy-
 37 dispersed structure of the low-energy ions during the northward IMF.

38 1 Introduction

39 The plasma sheet in the Earth's magnetosphere is an important target of magne-
 40 tospheric physics, since it is strongly related to geomagnetic activities through its role
 41 as the plasma reservoir. Previous research has revealed that the near-Earth plasma sheet
 42 becomes cold and dense under the northward interplanetary magnetic field (IMF) (e.g.,
 43 Zwolakowska et al., 1992; Zwolakowska & Popielawska, 1992; Terasawa et al., 1997;
 44 Borovsky et al., 1998; Nishino et al., 2002; Wing et al., 2005; Nagata et al., 2008). The
 45 formation of the cold-dense plasma sheet (CDPS) has been thought as a result of solar
 46 wind entry across the magnetopause and subsequent plasma transport inside the magneto-
 47 tail.

48 Several mechanisms have been proposed to explain the solar wind plasma entry
 49 across the magnetopause under the northward IMF, and some of them have been verified.
 50 In particular, under the strongly northward IMF condition, double-lobe reconnection (also
 51 known as magnetic reconnection poleward of the cusp) (e.g., Song & Russell, 1992; Li
 52 et al., 2005; Sorathia et al., 2019) and Kelvin-Helmholtz instability (e.g., Fairfield et al.,
 53 2000; Hasegawa et al., 2004) play an important role in solar wind plasma entry across the
 54 magnetopause. The solar wind entry across the magnetopause results in the formation of
 55 the low-latitude boundary layer (LLBL) filled with cold and dense plasma, and it possibly
 56 forms the CDPS in a wide region of the near-Earth magnetotail.

57 On the other hand, the plasma transport mechanism inside the magnetosphere under
 58 the northward IMF has not been well understood. Since the plasma flow in the near-Earth
 59 magnetotail under the northward IMF should reflect the transport mechanism of the cold-
 60 dense plasma, it is important to investigate the plasma flow velocity in the plasma sheet.
 61 Statistically, ion flows in the near-Earth plasma sheet during the geomagnetically quiet
 62 periods are quite stagnant with a slight earthward component (e.g., Angelopoulos et al.,
 63 1993). For most of the time, the ions in the CDPS adjacent to the LLBL slowly flow to-
 64 wards the Earth (Fujimoto et al., 1998).

65 The response time of the near-Earth plasma sheet to the solar wind during the north-
 66 ward IMF is confirmed to be longer than that during the southward IMF (e.g., Nagata et
 67 al., 2008). Based on the longer duration (\sim several hours) of the CDPS formation and the
 68 low bulk velocity in the near-Earth plasma sheet under the northward IMF, diffusive trans-

port in the plasma sheet has been proposed as a dominant mechanism in the magnetotail (Terasawa et al., 1997; Nagata et al., 2008; Wang et al., 2010). However, the CDPS occasionally appears in the midnight region only a few hours after the start of the strongly northward IMF period (Nishino, Fujimoto, Terasawa, et al., 2007), which suggests that non-diffusive plasma transport may work in the plasma sheet under the northward IMF.

In this paper we report on energy-dispersed low-energy ions in the field-aligned directions observed by the Magnetospheric Multiscale (MMS) mission spacecraft in the near-Earth magnetotail on the duskside under the strongly northward IMF. We will discuss possible mechanisms for generating energy dispersion in relation to the formation and temporal development of the CDPS in the flank of the magnetotail.

2 Instrumentation

We use ion and electron data from Fast Plasma Investigation (FPI) (Pollock et al., 2016) and magnetic field data from Fluxgate Magnetometer (FGM) (Russell et al., 2016) onboard MMS1, which is one of the four spacecraft in the MMS mission (Burch et al., 2016). The ion energy range of FPI for the event studied in this paper is from a few eV to 30 keV, which fully covered the typical energy of low-energy (cold) ions in the plasma sheet. Since burst-mode data were unavailable for the period of the current study, we use the fast survey-mode plasma data with a resolution of 4.5 s, which has no impact on the results presented in this paper. The four spacecraft were positioned at a distance of less than 20 km from each other, which is less than the ion kinetic scale. (The gyroradius of a 0.1-keV proton is ~ 70 km in a 20-nT magnetic field.) During the events, all four spacecraft observed almost identical ion signatures at the resolution of 4.5 s, and thus we use only MMS1 data in this study. The solar wind data from the Advanced Composition Explorer (ACE) and Wind spacecraft are referred to. The geocentric solar magnetospheric (GSM) coordinate system is used throughout.

3 Observations

Figure 1 presents an overview of MMS1 observations in the duskside magnetotail from 00:00 to 08:00 UT on August 4, 2017. For the first two hours, MMS1 remained in the lobe/mantle region in the northern hemisphere, which is characterised by a large B_X (Fig. 1a) and tailward plasma flows (Fig. 1f). CDPS observations continued for several hours between $\sim 02:00$ and $\sim 07:00$ UT. The omnidirectional ion energy-time (E-t) spectrogram illustrates the coexistence of high- and low-energy components (Fig. 1b), which is characteristic of the CDPS on the duskside under the northward IMF (Hasegawa et al., 2003; Wing et al., 2005; Nishino, Fujimoto, Ueno, Maezawa, et al., 2007). The electron E-t spectrogram (Fig. 1c) reveals that low-energy electrons (< 1 keV) were the main component of the CDPS. The solar wind conditions and the characteristics of the CDPS from 02:00 to 07:00 UT will be examined in the following.

The ion density and temperature in the CDPS were $\sim 4\text{--}6\text{ cm}^{-3}$ and 0.4–0.7 keV, respectively (Fig. 1d and e). The parallel ion temperature is higher than the perpendicular ion temperature, which is consistent with previous statistical results (Nishino, Fujimoto, Ueno, Maezawa, et al., 2007). The plasma beta (β , the ratio of thermal pressure to magnetic pressure) in the CDPS was mainly between 1 and 10, which is characteristic of the central plasma sheet. The bulk speed of the ion flows in the CDPS was very low (typically, below 50 km/s), which is consistent with the previous statistical results for geomagnetically quiet periods (e.g., Angelopoulos et al., 1993).

Solar wind data from ACE (Fig. 2a–e) and Wind (Fig. 2f–j) illustrate that the CDPS in the dusk magnetotail formed during a prolonged northward IMF. After 21:00 UT on 3 August, the IMF pointed weakly northward, and then it turned strongly northward at around 01:00 UT on 4 August as both B_X and B_Y decreased. The IMF strength for the

118 northward IMF period was higher than 10 nT. As the solar wind density data from ACE
 119 are available only for limited periods, we also use the data from Wind. The ACE and
 120 Wind spacecraft locations at 01:00 UT (which roughly corresponds to 02:00 UT at the
 121 Earth's magnetosphere when the solar wind convection is considered) were $(226, -21,$
 122 $-3)R_E$ and $(234, 98, -14)R_E$ in the GSM coordinate system, respectively, where the
 123 Earth's radius (R_E) is defined as 6,378 km. The trends of the prolonged northward IMF
 124 and high-density solar wind plasma were observed at both the ACE and Wind locations.
 125 When MMS1 observed the CDPS in the magnetotail, the solar wind speed and density
 126 at ACE were ~ 400 km/s and $20\text{--}40$ cm $^{-3}$, respectively. The solar wind dynamic pressure
 127 was as high as 6–12 nPa, and the large temporal variation was attributed to the density
 128 fluctuations. The solar wind flow had relatively large azimuthal and latitudinal velocity
 129 components; a negative V_Y until $\sim 05:00$ UT and a positive V_Z after $\sim 04:00$ UT were de-
 130 tected. These solar wind characteristics indicate the passage of the corotational interaction
 131 region around the Earth's magnetosphere.

132 At around 01:58 UT when MMS1 was located at $(-22.6, 9.6, 4.3)R_E$ in the GSM
 133 coordinate system, the spacecraft moved from the northern lobe/mantle region to the stag-
 134 nant CDPS region. Now we examine the ion E-t spectrograms in the directions parallel
 135 ($0^\circ\text{--}30^\circ$), perpendicular ($75^\circ\text{--}105^\circ$), and anti-parallel ($150^\circ\text{--}180^\circ$) to the magnetic field
 136 (Fig. 3b–d). Throughout the period of the CDPS, both the parallel and anti-parallel fluxes
 137 in the low-energy range (< 3 keV) were higher than the perpendicular flux. This observa-
 138 tion is consistent with Nishino et al.'s (2007a) report of parallel anisotropy of low-energy
 139 ions in the duskside CDPS under the strongly northward IMF.

140 In addition, we have found energy dispersions of low-energy ions in both the paral-
 141 lel and anti-parallel directions (indicated by black arrows in Fig. 3b and d) that typically
 142 started at 1–2 keV and ended at 0.1–0.3 keV. These energy-dispersed ions were detected
 143 on the closed field lines, which is evidenced by bi-directional distributions of the low-
 144 energy electrons (Fig. 3i and j). The path length of these energy-dispersed ions from the
 145 acceleration source to the observing location can be estimated by assuming the time-of-
 146 flight (TOF) effect (e.g., Kazama & Mukai, 2003). From the start of the CDPS obser-
 147 vation (at 01:57 UT) until 02:30 UT, the typical duration of the energy dispersion in the
 148 parallel direction was ~ 3 min (at 01:58, 02:18, 02:22, 02:23, and 02:27 UT). In the anti-
 149 parallel direction, faint energy dispersions with longer durations (~ 15 min) were observed
 150 at around 02:17 UT and 02:27 UT. This signature may demonstrate that these ions were in-
 151 jected from the magnetotail plasma sheet toward the lower altitude region and came back
 152 toward the spacecraft by the mirror reflection. However, because the magnetic field direc-
 153 tion changed within on a shorter timescale than the dispersion, we refrain from perform-
 154 ing further analysis for this event.

155 We focus on the energy-dispersion event in the parallel direction between 02:23
 156 and 02:26 UT (indicated by the thick arrow in Fig. 3b), when the dispersion signature was
 157 most obvious. As in previous studies (see Fig. 3 in Kazama and Mukai (2003) and Fig. 6
 158 in Varsani et al. (2017)), we plot spectrograms of the reciprocal speed (V^{-1}) of the ions
 159 with respect to time (Fig. 4e and f). The reciprocal speed linearly increased from 02:23 to
 160 02:26 UT, which is attributed to the TOF effect of the injected ions. By extrapolating the
 161 upper cutoff of the V^{-1} - t slope backward in time, the time of the injection is estimated
 162 to be around 02:22:30 UT. The path length (L) from the injection point to the spacecraft
 163 location is estimated as follows:

$$L = \frac{\Delta t}{(\Delta V)^{-1}} = \frac{120[\text{s}]}{0.055[\text{km}^{-1}\text{s}]} = 3.4R_E, \quad (1)$$

164 where 0.055 km $^{-1}$ s was used as the upper cutoff of V^{-1} at 02:24:30 UT and 120 s was
 165 used as the traveling time, although the estimation errors are relatively large.

166 We further investigate the ion distribution function during the energy-dispersion
 167 event by making a two-dimensional slice in the plane including the local magnetic field

168 direction. When drawing the slice, the bulk velocity perpendicular to the local magnetic
 169 field was subtracted in the velocity space. A slice in the middle of the event between
 170 02:24:29 and 02:24:34 UT reveals a cold ion beam parallel to the magnetic field (Fig. 5).
 171 The beam had a peak around 270 km/s with a lower energy cutoff at around 180 km/s at
 172 which the energy flux was roughly $1/e$ of the peak flux. The pitch angles of the beam
 173 ions were concentrated within 30° , with a broadened distribution up to 45° . The travel-
 174 ing time and path length from the injection point to the spacecraft location were estimated
 175 by a method described in Burch et al. (1982) that uses observed pitch-angle distributions
 176 and a geomagnetic field model. We compare the observed lower cutoff velocity of the en-
 177 ergy flux with the theoretically calculated velocity, by modifying several injection points
 178 and traveling times, and adopting the T96 model (Tsyganenko & Stern, 1996) as the ge-
 179 omagnetic field. The black rectangles in Fig. 5 denote the lower cutoff estimated from
 180 the Burch's method under assumptions of a traveling time of 110 s and a path length of
 181 $3.3 R_E$, for the pitch angles every 5° between 0° and 45° . Although this method was un-
 182 able to generate exact traveling times and path lengths for this event, the estimated values
 183 correspond with the observed lower cutoff velocity and thus are consistent with those ob-
 184 tained from the $V^{-1}-t$ spectrograms.

185 We use the T96 model to trace the magnetic field line to both the northern and
 186 southern polar regions. At 02:30 UT when MMS1 remained in the northern plasma sheet
 187 with a dominant positive B_X , the magnetic field line traced from the spacecraft's location
 188 toward the southern ionosphere crossed the neutral sheet $\sim 10 R_E$ tailward of the spacecraft
 189 (Fig. 6). It is plausible that the ion beams in the parallel (earthward) direction emanated
 190 directly from the source, while the anti-parallel ion beams were reflected at lower altitudes
 191 in the northern hemisphere and returned to the magnetotail. The interval of the dispersive
 192 signatures in the parallel direction was roughly several minutes, and short dispersions in
 193 the parallel direction were more frequently detected than longer faint dispersions in the
 194 anti-parallel direction. This difference in detection frequencies could indicate a depen-
 195 dence on distance from the acceleration source.

196 We next examine the CDPS that was continuously observed a few hours after the
 197 strongly northward IMF came to the Earth's magnetosphere. Between 04:00–06:00 UT,
 198 MMS1 remained in the CDPS where longer energy dispersions were observed in both the
 199 parallel and anti-parallel directions (Fig. 7). The ions signatures were similar to those in
 200 the preceding period, while B_Z dominated the magnetic field. The magnetic field strength
 201 and ion density in the CDPS were about 20 nT and 5 cm^{-3} , respectively, which gave a
 202 local Alfvén speed of $\sim 180 \text{ km/s}$.

203 We then focus on the energy dispersion event in the anti-parallel direction between
 204 04:30 and 04:44 UT (Fig. 8). As in the previous event, a linear increase was revealed in
 205 the reciprocal speed of the energy-dispersed ions. By extrapolating the slope of the linear
 206 increase, we estimated that an ion injection event occurred at around 04:20 UT. Using the
 207 inclination of the slope, and the path length (L) was estimated to be $54 R_E$ as follows:

$$L = \frac{\Delta t}{(\Delta V)^{-1}} = \frac{1200 [\text{s}]}{0.035 [\text{km}^{-1} \text{s}]} = 54 R_E . \quad (2)$$

208 The estimated path length indicates that the energy-dispersed ions were previously mirror
 209 reflected at lower altitudes.

210 Fig. 9a and b show two-dimensional slices of the ion distribution functions at 04:35:20 UT
 211 and 04:40:20 UT (also denoted by the dashed lines in Fig. 8). The bulk velocity perpen-
 212 dicular to the local magnetic field was subtracted from the original data. We focus on an
 213 observed ion beam in the anti-parallel direction corresponding to the energy dispersion
 214 in the E-t spectrogram. At 04:35:20 UT, the energy flux of this beam component had a
 215 peak around 490 km/s with an elongated shape in the perpendicular direction. The pitch
 216 angle of the ion beam ranged between 180° and $\sim 150^\circ$ with a broadened distribution in
 217 a crescent-like form. We calculated lower cutoff velocities using the Burch's method for

218 several combinations of injection points and traveling durations to identify those with a
 219 good fit with the observed distribution functions. The estimated values are the injection
 220 point of $5 R_E$ tailward of the MMS1 spacecraft and the injection event at 04:19:20 UT
 221 (i.e., a traveling time of 960 s). The rectangles in Fig. 9a denotes the cutoff velocities cal-
 222 culated for pitch angles at increments of 5° between 175° and 135° under the assumption
 223 of an injection point of $5 R_E$ tailward of MMS1 along the magnetic field line and the in-
 224 jection event at 04:19:20 UT.

225 Five minutes later at 04:40:20 UT, there was a decrease in both peak and cutoff
 226 speeds to 340 km/s and 280 km/s, respectively. A combination of the same injection point
 227 as above and a traveling time of 1260 s gave cutoff velocities that well fitted the obser-
 228 vations (Fig. 9b). This travelling time corresponds to the injection event at 04:19:20 UT,
 229 which roughly matches the event time estimated from the $V^{-1}-t$ slope. The path length
 230 of the mirror reflected ions (i.e., from the injection source via the mirror point to the ob-
 231 served location) is strongly contingent on the pitch angle. A calculation of path length
 232 using the T96 model for a pitch angle of 175° at the MMS1 spacecraft gives $54 R_E$, which
 233 is consistent with the estimation by the $V^{-1}-t$ slope. These ions were mirror reflected
 234 at $(-0.72, 0.88, 2.6) R_E$ in GSM where the magnetic field strength was 2510 nT. On the
 235 other hand, the path length for a pitch angle of 150° was calculated to be $38 R_E$: the loca-
 236 tion and the magnetic field strength of the mirror point were $(-6.7, 4.7, 5.2) R_E$ in GSM
 237 and 76 nT, respectively. The path length in this estimation is dependent solely on the loca-
 238 tion of the mirror point, as the same injection point is assumed for all pitch angles. We
 239 assumed that the pitch angle is precisely equal to 180° when the path length from the
 240 $V^{-1}-t$ slope in the anti-parallel direction was estimated. No contradiction exists between
 241 the shorter path length estimated for a pitch angle of 150° and the entire scenario of the
 242 injection and mirror reflection.

243 It is likely that the energy dispersion of low-energy ions generally occurs in the
 244 well-developed CDPS several hours after the start of the strongly northward IMF. The
 245 CDPS dominated by B_Z is consistent with the plasma sheet thickening and an increase
 246 in the total plasma content (Nishino et al., 2002; Fuselier et al., 2015). The prolonged
 247 presence of a large B_Z in the CDPS under the strongly northward IMF suggests that the
 248 magnetic field lines of the near-Earth magnetotail shifted from a tail-like shape to a less-
 249 stretched shape, which was reported in previous research by Petrukovich et al. (2003). If
 250 the large B_Z of the CDPS in this event is the result of the plasma sheet thickening under
 251 the strongly northward IMF, it is interesting to note that plasma sheet thickening and thus
 252 increased magnetotail plasma content are simultaneously observed with low-energy ion
 253 transport by injection.

254 For most of the time, the bulk ion speed in the CDPS was as low as ~ 50 km/s,
 255 which is consistent with previous statistical results (e.g., Angelopoulos et al., 1993) and
 256 event studies (e.g., Fujimoto et al., 1998). We note that even when energy dispersion oc-
 257 curs, both the parallel and perpendicular velocities are low. In the velocity moment calcu-
 258 lation, since the parallel and anti-parallel components negate each other, the low parallel
 259 velocity does not contradict the observed ion transport in the field-aligned direction.

260 4 Summary and Discussion

261 We identified energy-dispersed low-energy ions in the CDPS in the duskside mag-
 262 netotail under the strongly northward IMF and analyzed injection points in two ways, that
 263 is, by assuming the TOF effect and by using information of pitch angle dispersions. Dur-
 264 ing the first event, the energy-dispersed ions in the direction parallel to the magnetic field
 265 were deemed to have originated from the tail flank plasma sheet several R_E tailward of the
 266 MMS1 spacecraft's location. During the second event, a longer duration of the ion energy
 267 dispersion in the anti-parallel direction was evident, which indicates that these ions once

268 traveled along the magnetic field toward the ionosphere and were mirror reflected at a low
269 altitude back to the magnetotail plasma sheet.

270 The energy-dispersed ions in the field-aligned directions are not inconsistent with
271 the stagnant plasma flows in the CDPS under the northward IMF. This is because the ion
272 velocities in the parallel and anti-parallel directions were negated and thus did not exist in
273 the bulk velocity, i.e., the low bulk velocity obtained from the moment calculation did not
274 necessarily indicate the dominance of diffusive plasma transport.

275 The observed energy dispersions mean that some acceleration mechanisms would
276 work in the tail flank region. Possible candidates for the acceleration mechanism of the
277 energy-dispersed ions are (1) magnetic reconnection in well-developed Kelvin-Helmholtz
278 vortices (e.g., Takagi et al., 2006; Nishino, Fujimoto, Ueno, Mukai, & Saito, 2007; Naka-
279 mura et al., 2017), (2) tension force of the closed magnetic field lines (Fujimoto et al.,
280 1996), and (3) additional mechanisms including small magnetic reconnection in the turbu-
281 lent plasma sheet (Borovsky & Funsten, 2003).

282 During the events reported in this study, the magnetopause under the strongly north-
283 ward IMF was likely to be Kelvin-Helmholtz unstable to generate vortical structures flow-
284 ing tailward. The intervals of energy dispersive signatures were a few to several minutes,
285 which is similar to the period of the Kelvin-Helmholtz vortices in the magnetotail flanks
286 (e.g., Nishino et al., 2011). In previous studies, ion beams observed in the LLBL under
287 the northward IMF have been interpreted in the context of Kelvin-Helmholtz instability
288 (Nishino, Fujimoto, Ueno, Mukai, & Saito, 2007; Taylor & Lavraud, 2008). Stenuit et
289 al. (2001, 2002) reported the detection of energy-dispersed ions in the LLBL at the low-
290 altitude region under the northward IMF, and suggested that Kelvin-Helmholtz instability
291 at the tail magnetopause is related to the generation of energy-dispersed ions. The speed
292 of the ion beams in the LLBL that were possibly accelerated inside the Kelvin-Helmholtz
293 vortices is estimated to be in the order of the reconnection Alfvén speed (e.g., Ma et al.,
294 2017). The LLBL was not detected directly in this study, but the local Alfvén speed in
295 the CDPS was around 180 km/s (for a density of 5 cm^{-3} and a magnetic field strength of
296 20 nT), which is below the observed maximum speed of the energy-dispersed ions (typi-
297 cally, 400–500 km/s). However, if magnetic reconnection occurs in the lower density re-
298 gion closer to the plasma sheet boundary layer, the higher Alfvén speed may explain the
299 maximum speed of the ion beams.

300 A scenario of the tension force of the closed field lines in the LLBL or in the CDPS
301 adjacent to the LLBL is considered. The closed field lines in the LLBL/CDPS are stretched
302 tailward by viscous interactions with the magnetosheath plasma, and finally return toward
303 the Earth by the magnetic tension force (Fujimoto et al., 1996). This process may accel-
304 erate the ions toward the Earth and would be evidenced by the occurrence of fast bulk
305 flows. However, because fast earthward flows were undetected by MMS during the events
306 in this study, it is unlikely that magnetic tension force is instrumental in generating the
307 observed energy-dispersed structures.

308 Considering the origins of the cold-dense plasma, although double-lobe reconnection
309 is the most plausible mechanism for capturing the magnetosheath plasma into the Earth's
310 magnetosphere, formation of the lobe/mantle region is also a potential candidate for the
311 entry process. MMS1 data before 01:58 UT confirm the entry of large amounts of cold
312 ions into the magnetotail via the lobe/mantle region during the northward IMF with an
313 enhanced IMF B_y . It is possible that the low-energy ions from the lobe/mantle region are
314 the partial source of the energy-dispersed ions detected in the plasma sheet after 01:58 UT,
315 since the detection of the CDPS by MMS1 started in the outer plasma sheet close to the
316 northern lobe, as indicated by the large B_x component.

317 We discuss the possible relationship between energy-dispersed ions and the magnetosphere-
318 ionosphere coupling under the northward IMF. Stenuit et al. (2002) proposed a connection

319 between the energy-dispersed ions at a low altitude and the Kelvin-Helmholtz instability
320 at the tail magnetopause and demonstrated outflows of ionospheric oxygen ions under the
321 northward IMF. Wang et al. (2019) examined the CDPS events observed by MMS in the
322 magnetotail and DMSP-F18 in a low-altitude orbit and found increases in the density of
323 oxygen ions (O^+) of ionospheric origin at both locations under the northward IMF. Their
324 research revealed signatures of kinetic Alfvén waves that are capable of accelerating elec-
325 trons in the field-aligned direction, and they discussed that observed electrons injected
326 from the magnetosphere into the ionosphere playing a key role in the outflow of oxygen
327 ions from the ionosphere to the CDPS. The events in the current study was also analyzed
328 by Wang et al. (2019), i.e., the energy-dispersed ions in the CDPS coincided with the in-
329 crease in the oxygen ions from the ionosphere. It is worth noting that both kinetic Alfvén
330 waves and ion injection can be caused by magnetic reconnection in the Kelvin-Helmholtz
331 vortices. The major carrier of field-aligned current may be electrons accelerated by kinetic
332 Alfvén waves, which is consistent with the present study's observation of the low ion bulk
333 speed in the parallel direction. Yokoyama et al.'s (2020) recent observational study ana-
334 lyzed low-altitude satellite data and proposed a generation mechanism of mesoscale field-
335 aligned currents in the LLBL on the duskside during northward IMF periods. Their ob-
336 servation of the 630-nm auroral emission in the upward field-aligned current regions indi-
337 cates that the major carrier of the field-aligned currents under the northward IMF is elec-
338 trons precipitating into the ionosphere. However, because the present study was conducted
339 for the stagnant CDPS and not for the LLBL with tailward flows, further investigations
340 are required.

341 The energy dispersion of the low-energy ions in the current study occurred under
342 a condition of high-density solar wind. Although the effect of solar wind density on the
343 occurrence of the energy dispersion of the low-energy ions remains unclear, other CDPS
344 events with ion energy dispersion under conditions of the strongly northward IMF and
345 moderate solar wind density (data not shown here) have been identified. Therefore, the au-
346 thors consider that the field-aligned transport of low-energy ions in the near-Earth plasma
347 sheet generally occurs under the strongly northward IMF. However, further study is re-
348 quired into detailed mechanisms of ion acceleration under the strongly northward IMF and
349 plasma transport under the weakly northward IMF. Further research will also explore the
350 low-energy ion signatures in the CDPS in the dawn magnetotail as well as in the dawn
351 LLBL under the strongly northward IMF.

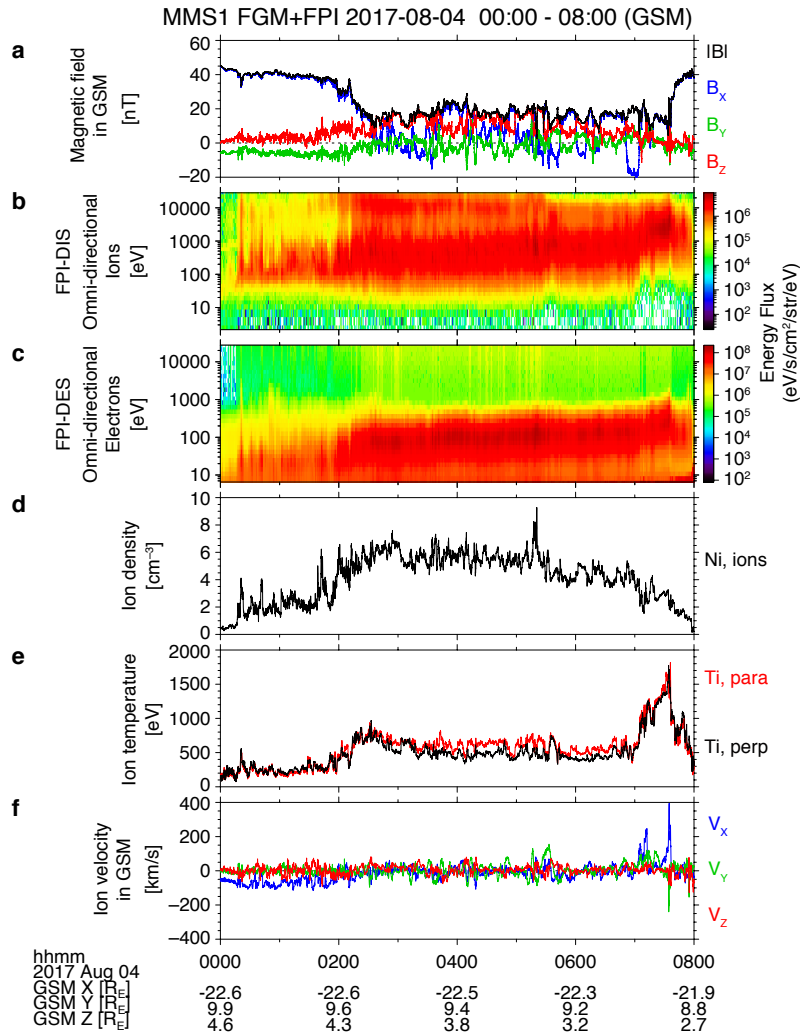


Figure 1. An overview of MMS1 observations between 00:00–08:00 UT on August 4, 2017. From the top: (a) magnetic field, (b) omnidirectional ion energy-time spectrogram, (c) omnidirectional electron energy-time spectrogram, (d) ion density, (e) parallel (red) and perpendicular (black) ion temperatures, and (f) ion velocity.

352 Acknowledgments

353 The authors are grateful to the entire MMS team and instrument leads for data ac-
 354 cess and support. Craig J. Pollock, Thomas E. Moore, James L. Burch, Jean-Andre Sauvaud,
 355 William R. Paterson, John Dorelli, Daniel Gershman, Conrad Schiff, Levon Avanov, Benoit
 356 Lavraud, Michael Chandler and Victoria Coffey are acknowledged for providing instru-
 357 mentation and data production/quality for the FPI instrument. The authors gratefully ac-
 358 knowledge the development team of the Space Physics Environment Data Analysis System
 359 (SPEDAS) software and thank the principal investigators of the ACE and Wind spacecraft
 360 for providing solar wind data through CDAWeb at NASA. Finally, Kazushi Asamura and
 361 Masaki Fujimoto are acknowledged for providing fruitful discussions.

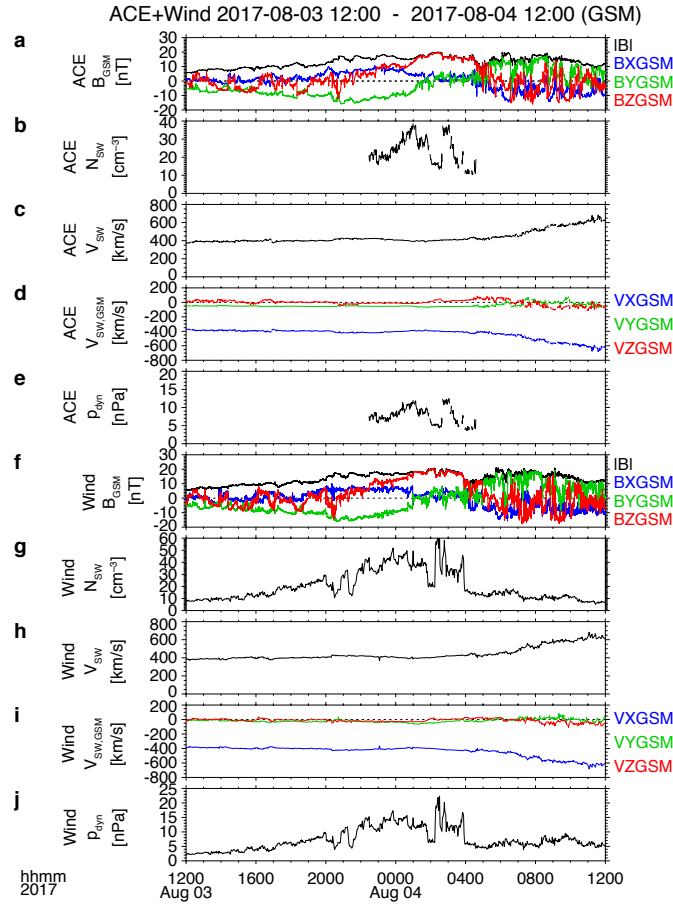


Figure 2. Solar wind data from ACE and Wind for 24 hours from 12:00 UT on August 3, 2017. From the top, (a) magnetic field, (b) ion density, (c) ion bulk speed, (d) ion flow vector, and (e) dynamic pressure from ACE. (f-j) Data from Wind are plotted in the same format as the ACE data.

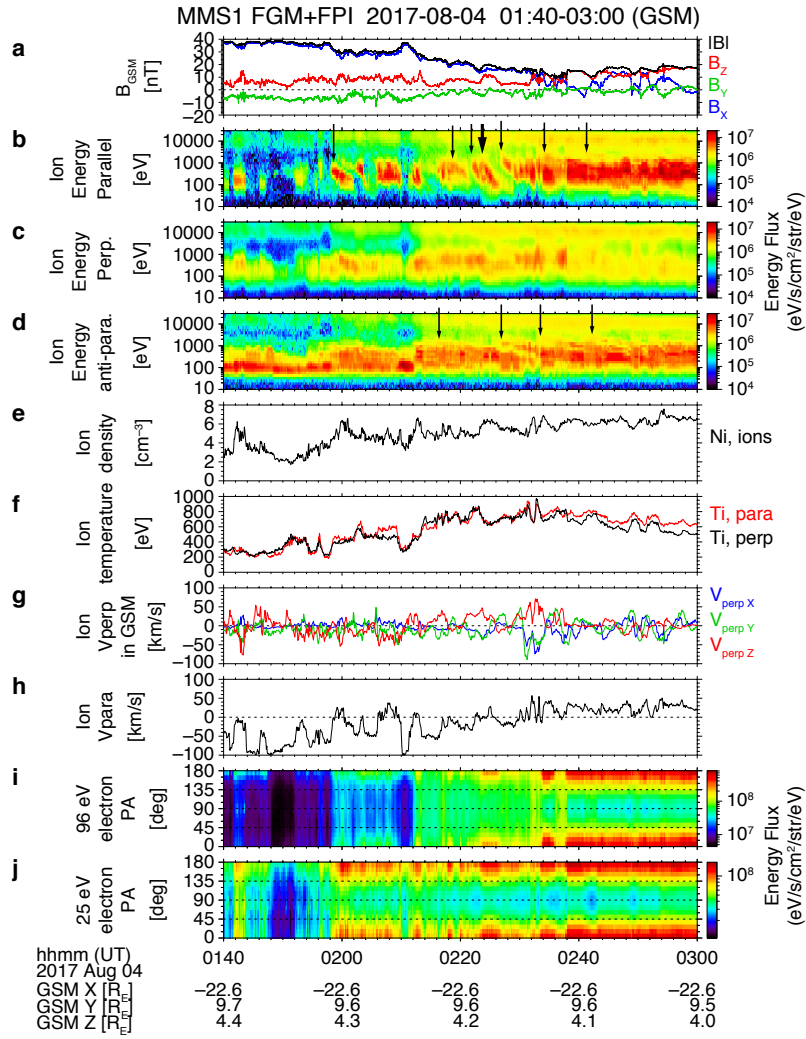


Figure 3. MMS1 observations between 01:40–03:00 UT on August 4, 2017. (a) Magnetic field, (b–d) ion energy-time spectrograms parallel, perpendicular, and anti-parallel to the magnetic field, (e) ion density, (f) ion parallel and perpendicular temperatures, (g) bulk ion velocity in the direction perpendicular to the local magnetic field, (h) bulk ion velocity in the parallel direction, (i) 96-eV electron pitch-angle distribution and (j) 25-eV electron pitch-angle distribution. Each arrow in the ion energy-time spectrograms indicates the beginning of energy dispersion. The thick arrow corresponds to the dispersion event analysed in detail in the main text.

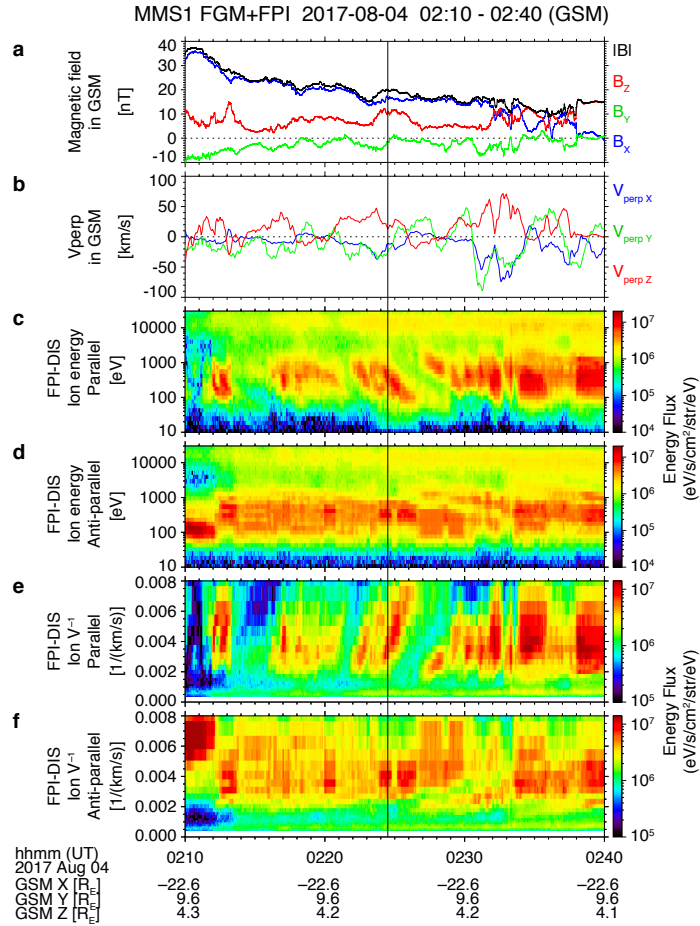


Figure 4. Energy-time spectrograms and reciprocal speed (V^{-1})-time spectrograms between 02:10–02:40 UT. (a) Magnetic field, (b) bulk ion velocity perpendicular to the magnetic field, (c and d) ion E-t spectrograms parallel and anti-parallel to the magnetic field, (e and f) reciprocal speed-time spectrograms in parallel and anti-parallel directions. A vertical dashed line marks the time when a two-dimensional slice of ion distribution function in Fig. 5 was taken.

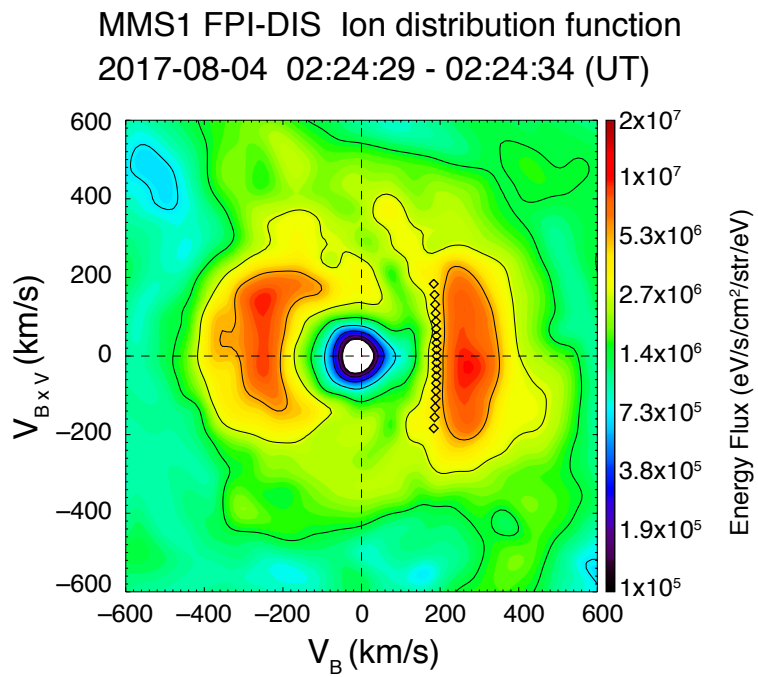


Figure 5. Two-dimensional slice of ion distribution function between 02:24:29–02:24:34 UT. The horizontal axis is the local magnetic field direction. The black rectangles show the lower cutoff of the distribution function of the ion beam for the pitch angles every 5° from 0° to 45° calculated using the Burch’s method (Burch et al., 1982).

2017-08-04 02:20 UT Magnetic field model (Tsyganenko 1996 in GSM)

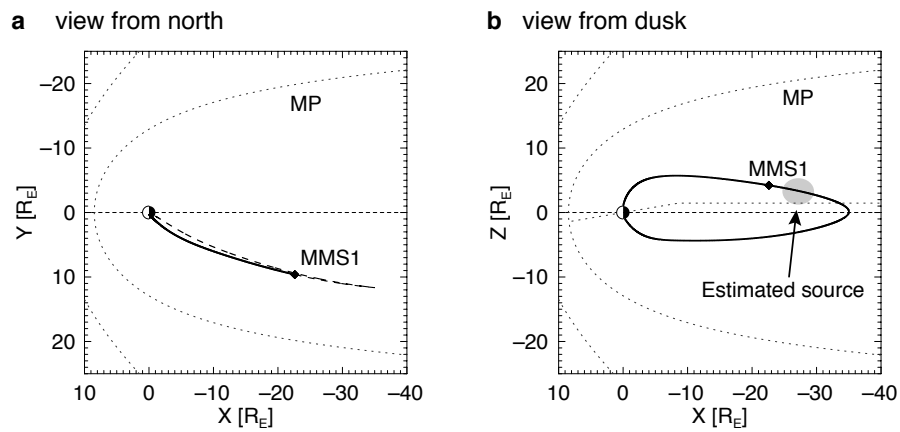


Figure 6. Traced magnetic field line at MMS1 using the T96 model at 02:20 UT. In the left panel, a solid (dotted) curve shows the magnetic field line traced from the MMS1 location toward the northern (southern) polar region. A dotted parabolic curve indicated by ‘MP’ is the modelled magnetopause location under a high solar wind dynamic pressure of 7.0 nPa (Shue et al., 1998). A gray region illustrates a roughly estimated source of the energy-dispersed ions.

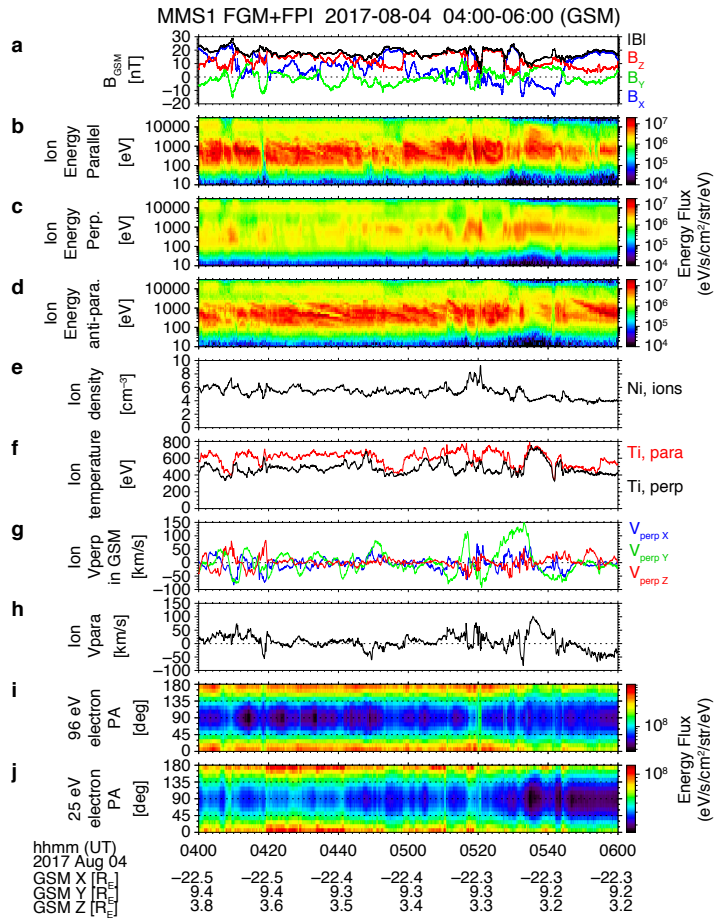


Figure 7. MMS1 observations between 04:00–06:00 UT on August 4, 2017 in the same format as Fig. 3.

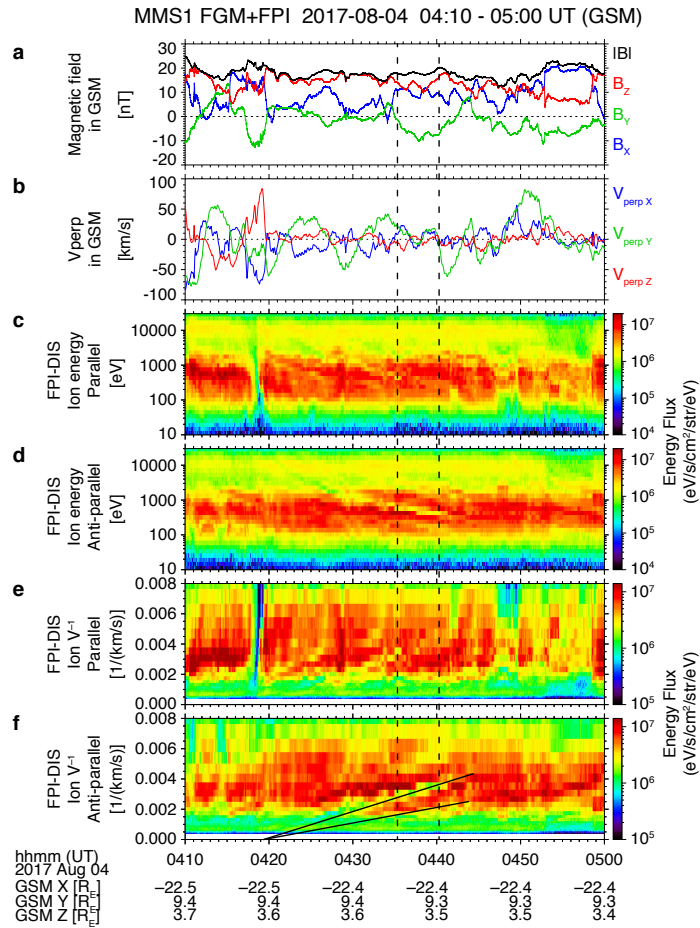
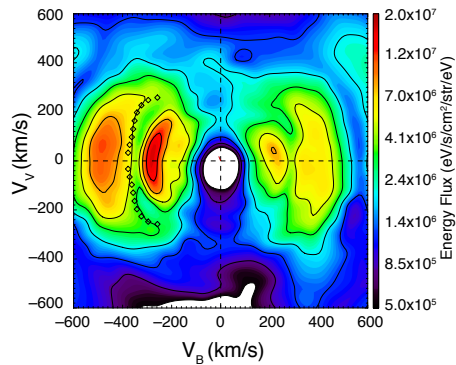


Figure 8. MMS1 data between 04:10–05:00 UT in the same format as Fig. 4. Two vertical lines correspond to the data presented in Fig. 9.

MMS1/FPI-DIS Ion distribution functions

(a) 04:35:17 – 04:35:22 (UT)



(b) 04:40:19 – 04:40:23 (UT)

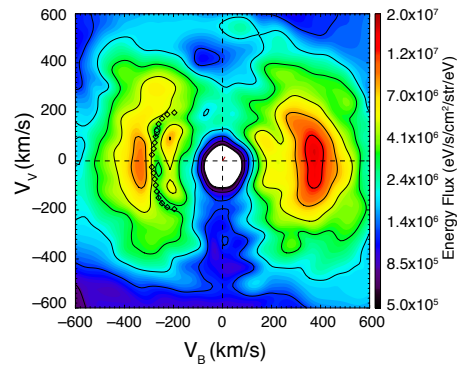


Figure 9. Two-dimensional slices of the ion distribution functions (a) between 04:35:17–04:35:22 UT and (b) between 04:40:19–04:40:23 UT. The black rectangles show the lower-energy cutoff of the distribution function of the ion beam for the pitch angles every 5° from 175° to 135° calculated using the Burch’s method (Burch et al., 1982).

362 MMS data are available from <https://lasp.colorado.edu/mms/sdc/public/>. Solar wind
 363 data from ACE and Wind were provided by NASA’s CDAWeb (<https://cdaweb.gsfc.nasa.gov/>).
 364 Data analysis was performed using SPEDAS V3.1 (see Angelopoulos et al. (2019) in de-
 365 tail).

366 This research was supported by the NASA MMS mission in association with NASA
 367 contract NNG04EB99C. Institut de Recherche en Astrophysique et Planétologie (IRAP)
 368 contributions to MMS FPI were supported by Centre National d’Études Spatiales (CNES)
 369 and Centre National de la Recherche Scientifique (CNRS). The work of MNN was sup-
 370 ported by JSPS KAKENHI Grant Number 19K03947, and the work of TN at ISAS/JAXA
 371 was supported by MEXT/JSPS KAKENHI Grant Number 17H06140.

372 References

- 373 Angelopoulos, V., Cruce, P., Drozdov, A., Grimes, E. W., Hatzigeorgiu, N., King, D. A.,
 374 ... Schroeder, P. (2019). *The Space Physics Environment Data Analysis System*
 375 (*SPEDAS*). doi: 10.1007/s11214-018-0576-4
 376 Angelopoulos, V., Kennel, C. F., Coroniti, F. V., Pellat, R., Spence, H. E., Kivelson, M. G.,
 377 ... Russell, C. T. (1993, aug). Characteristics of ion flow in the quiet state of the inner
 378 plasma sheet. *Geophysical Research Letters*, 20(16), 1711–1714. Retrieved from
 379 <http://doi.wiley.com/10.1029/93GL00847> doi: 10.1029/93GL00847
 380 Borovsky, J. E., & Funsten, H. O. (2003). MHD turbulence in the Earth’s plasma sheet:
 381 Dynamics, dissipation, and driving. *Journal of Geophysical Research: Space Physics*.
 382 doi: 10.1029/2002JA009625
 383 Borovsky, J. E., Thomsen, M. F., & Elphic, R. C. (1998). The driving of the plasma sheet

- 384 by the solar wind. *Journal of Geophysical Research: Space Physics*. doi: 10.1029/
385 97ja02986
- 386 Burch, J. L., Moore, T. E., Torbert, R. B., & Giles, B. L. (2016). *Magnetospheric Multiscale*
387 *Overview and Science Objectives*. doi: 10.1007/s11214-015-0164-9
- 388 Burch, J. L., Reiff, P. H., Heelis, R. A., Winningham, J. D., Hanson, W. B., Gurgiolo, C., ...
389 Barfield, J. N. (1982). Plasma injection and transport in the mid- altitude polar cusp.
390 *Geophysical Research Letters*. doi: 10.1029/GL009i009p00921
- 391 Fairfield, D. H., Otto, A., Mukai, T., Kokubun, S., Lepping, R. P., Steinberg, J. T., ... Ya-
392 mamoto, T. (2000). Geotail observations of the Kelvin-Helmholtz instability at the
393 equatorial magnetotail boundary for parallel northward fields. *Journal of Geophysical*
394 *Research: Space Physics*. doi: 10.1029/1999ja000316
- 395 Fujimoto, M., Nishida, A., Mukai, T., Saito, Y., Yamamoto, T., & Kokubun, S. (1996).
396 Plasma entry from the flanks of the near-Earth magnetotail: GEOTAIL observations
397 in the dawnside LLBL and the plasma sheet. *Journal of Geomagnetism and Geoelec-*
398 *tricity*. doi: 10.5636/jgg.48.711
- 399 Fujimoto, M., Terasawa, T., Mukai, T., Saito, Y., Yamamoto, T., & Kokubun, S. (1998).
400 Plasma entry from the flanks of the near-Earth magnetotail: Geotail observations.
401 *Journal of Geophysical Research: Space Physics*. doi: 10.1029/97ja03340
- 402 Fuselier, S. A., Dayeh, M. A., Livadiotis, G., McComas, D. J., Ogasawara, K., Valek, P., ...
403 Petrinc, S. M. (2015). Imaging the development of the cold dense plasma sheet.
404 *Geophysical Research Letters*. doi: 10.1002/2015GL065716
- 405 Hasegawa, H., Fujimoto, M., Maezawa, K., Saito, Y., & Mukai, T. (2003). Geotail obser-
406 vations of the dayside outer boundary region: Interplanetary magnetic field control
407 and dawn-dusk asymmetry. *Journal of Geophysical Research: Space Physics*. doi:
408 10.1029/2002JA009667
- 409 Hasegawa, H., Fujimoto, M., Phan, T. D., Rème, H., Balogh, A., Dunlop, M. W., ... Tan-
410 dokoro, R. (2004). Transport of solar wind into Earth's magnetosphere through
411 rolled-up Kelvin-Helmholtz vortices. *Nature*. doi: 10.1038/nature02799
- 412 Kazama, Y., & Mukai, T. (2003). Multiple energy-dispersed ion signatures in the near-
413 Earth magnetotail: Geotail observation. *Geophysical Research Letters*. doi: 10.1029/
414 2002GL016637
- 415 Li, W., Raeder, J., Dorelli, J., Øieroset, M., & Phan, T. D. (2005). Plasma sheet formation
416 during long period of northward IMF. *Geophysical Research Letters*. doi: 10.1029/
417 2004GL021524
- 418 Ma, X., Delamere, P., Otto, A., & Burkholder, B. (2017). Plasma transport driven by the
419 three-dimensional Kelvin-Helmholtz instability. *Journal of Geophysical Research:*
420 *Space Physics*. doi: 10.1002/2017JA024394
- 421 Nagata, D., MacHida, S., Ohtani, S., Saito, Y., & Mukai, T. (2008). Solar wind control of
422 plasma number density in the near-Earth plasma sheet: Three-dimensional structure.
423 *Annales Geophysicae*. doi: 10.5194/angeo-26-4031-2008
- 424 Nakamura, T. K., Hasegawa, H., Daughton, W., Eriksson, S., Li, W. Y., & Nakamura, R.
425 (2017). Turbulent mass transfer caused by vortex induced reconnection in collisionless
426 magnetospheric plasmas. *Nature Communications*. doi: 10.1038/s41467-017-01579
427 -0
- 428 Nishino, M. N., Fujimoto, M., Terasawa, T., Ueno, G., Maezawa, K., Mukai, T., & Saito, Y.
429 (2007). Geotail observations of temperature anisotropy of the two-component protons
430 in the dusk plasma sheet. *Annales Geophysicae*. doi: 10.5194/angeo-25-769-2007
- 431 Nishino, M. N., Fujimoto, M., Ueno, G., Maezawa, K., Mukai, T., & Saito, Y. (2007). Geo-
432 tail observations of two-component protons in the midnight plasma sheet. *Annales*
433 *Geophysicae*. doi: 10.5194/angeo-25-2229-2007
- 434 Nishino, M. N., Fujimoto, M., Ueno, G., Mukai, T., & Saito, Y. (2007). Origin of temper-
435 ature anisotropies in the cold plasma sheet: Geotail observations around the Kelvin-
436 Helmholtz vortices. *Annales Geophysicae*. doi: 10.5194/angeo-25-2069-2007
- 437 Nishino, M. N., Hasegawa, H., Fujimoto, M., Saito, Y., Mukai, T., Dandouras, I., ...
438 Schwartz, S. J. (2011). A case study of Kelvin-Helmholtz vortices on both flanks

- 439 of the Earth's magnetotail. *Planetary and Space Science*. doi: 10.1016/j.pss.2010.03
 440 .011
- 441 Nishino, M. N., Terasawa, T., & Hoshino, M. (2002). Increase of the tail plasma content
 442 during the northward interplanetary magnetic field intervals: Case studies. *Journal of*
 443 *Geophysical Research: Space Physics*. doi: 10.1029/2002JA009268
- 444 Petrukovich, A. A., Baumjohann, W., Nakamura, R., Balogh, A., Mukai, T., Glassmeier,
 445 K. H., ... Klecker, B. (2003). Plasma sheet structure during strongly northward IMF.
 446 *Journal of Geophysical Research: Space Physics*. doi: 10.1029/2002JA009738
- 447 Pollock, C., Moore, T., Jacques, A., Burch, J., Gliese, U., Saito, Y., ... Zeuch, M. (2016).
 448 *Fast Plasma Investigation for Magnetospheric Multiscale*. doi: 10.1007/s11214-016
 449 -0245-4
- 450 Russell, C. T., Anderson, B. J., Baumjohann, W., Bromund, K. R., Dearborn, D., Fischer,
 451 D., ... Richter, I. (2016). *The Magnetospheric Multiscale Magnetometers*. doi:
 452 10.1007/s11214-014-0057-3
- 453 Shue, J.-H., Song, P., Russell, C. T., Steinberg, J. T., Chao, J. K., Zastenker, G., ... Kawano,
 454 H. (1998). Magnetopause location under extreme solar wind conditions. *Journal of*
 455 *Geophysical Research: Space Physics*. doi: 10.1029/98ja01103
- 456 Song, P., & Russell, C. T. (1992). Model of the formation of the low-latitude boundary
 457 layer for strongly northward interplanetary magnetic field. *Journal of Geophysical*
 458 *Research*. doi: 10.1029/91ja02377
- 459 Sorathia, K. A., Merkin, V. G., Ukhorskiy, A. Y., Allen, R. C., Nykyri, K., & Wing, S.
 460 (2019). Solar Wind Ion Entry Into the Magnetosphere During Northward IMF. *Jour-*
 461 *nal of Geophysical Research: Space Physics*. doi: 10.1029/2019JA026728
- 462 Stenuit, H., Fujimoto, M., Fuselier, S. A., Sauvaud, J. A., Wing, S., Fedorov, A., ... Peder-
 463 sen, A. (2002). Multispacecraft study on the dynamics of the dusk-flank magneto-
 464 sphere under northward IMF: 10-11 January 1997. *Journal of Geophysical Research:*
 465 *Space Physics*. doi: 10.1029/2002JA009246
- 466 Stenuit, H., Sauvaud, J. A., Delcourt, D. C., Mukai, T., Kokubun, S., Fujimoto, M., ... Lep-
 467 ping, R. P. (2001). A study of ion injections at the dawn and dusk polar edges of
 468 the auroral oval. *Journal of Geophysical Research: Space Physics*. doi: 10.1029/
 469 2001ja900060
- 470 Takagi, K., Hashimoto, C., Hasegawa, H., Fujimoto, M., & TanDokoro, R. (2006). Kelvin-
 471 Helmholtz instability in a magnetotail flank-like geometry: Three-dimensional MHD
 472 simulations. *Journal of Geophysical Research: Space Physics*. doi: 10.1029/
 473 2006JA011631
- 474 Taylor, M. G., & Lavraud, B. (2008). Observation of three distinct ion populations at the
 475 Kelvin-Helmholtz-unstable magnetopause. *Annales Geophysicae*. doi: 10.5194/angeo
 476 -26-1559-2008
- 477 Terasawa, T., Fujimoto, M., Mukai, T., Shinohara, I., Saito, Y., Yamamoto, T., ... Lepping,
 478 R. P. (1997). Solar wind control of density and temperature in the near-Earth plasma
 479 sheet: WIND/GEOTAIL collaboration. *Geophysical Research Letters*. doi: 10.1029/
 480 96GL04018
- 481 Tsyganenko, N. A., & Stern, D. P. (1996). Modeling the global magnetic field of the large-
 482 scale Birkeland current systems. *Journal of Geophysical Research: Space Physics*.
 483 doi: 10.1029/96ja02735
- 484 Varsani, A., Nakamura, R., Sergeev, V. A., Baumjohann, W., Owen, C. J., Petrukovich,
 485 A. A., ... Ergun, R. (2017). Simultaneous Remote Observations of Intense Reconnec-
 486 tion Effects by DMSP and MMS Spacecraft During a Storm Time Substorm. *Journal*
 487 *of Geophysical Research: Space Physics*. doi: 10.1002/2017JA024547
- 488 Wang, C. P., Fuselier, S. A., Hairston, M., jia Zhang, X., Zou, S., Avanov, L. A., ... Bortnik,
 489 J. (2019). Event Studies of O+ Density Variability Within Quiet-Time Plasma Sheet.
 490 *Journal of Geophysical Research: Space Physics*. doi: 10.1029/2019JA026644
- 491 Wang, C. P., Lyons, L. R., Nagai, T., Weygand, J. M., & Lui, A. T. (2010). Evolution of
 492 plasma sheet particle content under different interplanetary magnetic field conditions.
 493 *Journal of Geophysical Research: Space Physics*. doi: 10.1029/2009JA015028

- 494 Wing, S., Johnson, J. R., Newell, P. T., & Meng, C. I. (2005). Dawn-dusk asymmetries,
495 ion spectra, and sources in the northward interplanetary magnetic field plasma sheet.
496 *Journal of Geophysical Research: Space Physics*. doi: 10.1029/2005JA011086
- 497 Zwolakowska, D., Koperski, P., & Popielawska, B. (1992). Plasma populations in the tail
498 during northward IMF. *Proceedings of the international conference on substorms*
499 *(ICS-1), Kiruna, Sweden (ESA SP-335)*, 57–62.
- 500 Zwolakowska, D., & Popielawska, B. (1992). Tail Plasma Domains and the Auroral Oval —
501 Results of Mapping Based on the Tsyganenko 1989 Magnetosphere Model. *Journal of*
502 *Geomagnetism and Geoelectricity*(44), 1145–1158. doi: 10.5636/jgg.44.1145